# Excited States and Excitonic Interactions in Prototypic Polycyclic Aromatic Hydrocarbon Dimers as Models for Graphitic Interaction in Carbon Dots



| | |
|---|---|
| Journal: | *Physical Chemistry Chemical Physics* |
| Manuscript ID | CP-ART-01-2019-000635.R1 |
| Article Type: | Paper |
| Date Submitted by the Author: | 25-Feb-2019 |
| Complete List of Authors: | Shi, Baimei; Tianjin University<br>Nachtigallova, Dana; Academy of Sciences of the Czech Republic,<br>Aquino, Adelia; University of Vienna,<br>Machado, Francisco; Instituto Tecnológico de Aeronáutica, Departamento de Química<br>Lischka, Hans; University of Vienna, Institute for Theoretical Chemistry and Structural Biology |
| | |

# Excited States and Excitonic Interactions in Prototypic Polycyclic Aromatic Hydrocarbon Dimers as Models for Graphitic Interaction in Carbon Dots

Baimei Shi,[a] Dana Nachtigallová,*[,b,c] Adélia J. A. Aquino,[a] Francisco B. C. Machado,[d] and Hans Lischka[a,*]

[a] School of Pharmaceutical Science and Technology, Tianjin University, Tianjin 300072, P.R. China

[b] Institute of Organic Chemistry and Biochemistry v.v.i., The Czech Academy of Sciences, Flemingovo nám. 2, 16610 Prague 6, Czech Republic

[c] Regional Centre of Advanced Technologies and Materials, Palacký University, 78371 Olomouc, Czech Republic

[d] Departamento de Química, Instituto Tecnológico de Aeronáutica, São José dos Campos 12228-900, São Paulo, Brazil

Electronic supplementary information (ESI) available. See DOI:

Email: dana.nachtigallova@marge.uochb.cas.cz, hans.lischka@univie.ac.at

**Abstract**

The study of electronically excited states of stacked polycyclic aromatic hydrocarbons (PAHs) is of great interest due to promising applications of these compounds as luminescent carbon nanomaterials such as graphene quantum dots (GQDs) and carbon dots (CDs). In this study, the excited states and excitonic interactions are described in detail based on four CD model dimer systems of pyrene, coronene, circum-1-pyrene and circum-1-coronene, respectively. Two multi-reference methods, DFT/MRCI and SC-NEVPT2, and two single-reference methods, ADC(2) and CAM-B3LYP have been used for excited states calculations. The DFT/MRCI method has been used as benchmark method to evaluate the performance of the other ones. All methods produce useful lists of excited states. However, an overestimation of excitation energies and inverted ordering of states, especially concerning the bright HOMO-LUMO excitation, is observed. In the pyrene-based systems, the first bright state appears among the first four states whereas the number of dark states is significantly larger for the coronene-based systems. Fluorescence emission properties are addressed by means of geometry optimization in the $S_1$ state. Inter sheet distances for the $S_1$ state decrease in comparison to the corresponding ground-state values. These reductions are largest for the pyrene dimer and decrease significantly for the larger dimers. Several minima have been determined on the $S_1$ energy surface for most of the dimers. The largest variability in emission energies is found for the pyrene dimer whereas in the other cases a more regular behavior of the emission spectra is observed.

**Key words:** UV-absorption, fluorescence emission, quantum chemical methods, multireference calculations

# 1 Introduction

Excited state aggregates of polycyclic aromatic species which are building blocks of graphene quantum dots (GQDs) and carbon dots (CDs) are currently extensively studied systems as promising luminescent carbon nanomaterials[1] due to their potential applications in photonics and optoelectronics, organic devices, singlet fission processes, and bio- and medical applications.[2-7] Understanding and controlling the origin of the photoluminescence of GQDs and CDs which can help in a rational design of carbon-based materials was the subject of experimental and computational research (for recent studies see e.g. [8-10]). GQDs can be characterized as larger polycyclic aromatic hydrocarbons (PAHs) which obtain their discrete absorption and emission spectra due to their quantum confinement as compared to graphene sheets.[11] CDs are more complex 3-dimensional systems which contain as important components graphitic regions responsible for their photoluminescence properties.[12] Due to the aggregation of PAHs in the graphitic regions of stacked sheets, the optical properties often resemble those of excimers (excited state dimers of two identical monomers) or exciplexes (excited state complex of two non-identical monomers), complexes weakly associated in the ground state, but strongly interacting in the excited states.[13, 14] Potential applications of these associates, including those in CDs were already suggested in several studies[15-21] and their optical properties were investigated also computationally using model systems.[22-24]

The first experimentally observed pyrene excimer,[25] as one of the basic PAH excimer models, received great attention as the basis for a wide range of applications in optoelectronics.[26] It is characterized by a singly red-shifted, broad and structureless fluorescence band whose intensity depends on the pyrene concentration.[27-29] The band was predicted to originate from the dimer state which results from the splitting of monomer bright $L_a$ states.[25, 30] The dynamics of the pyrene excimer formation was a subject of recent computational and experimental studies.[31, 32] The theory which underlines the excimer character was formulated by Scholes and Ghiggino[33] based on the seminal work of Förster.[30] Monomers interact via their transition dipole moments and charge transfer interactions leading to excitonic resonance (ER) and charge resonance (CR)[34] effects. Both terms and their mixing contribute to the excimer stability.[33] In terms of monomer 1 and 2, excited states with the excitation located on one of the monomers form states described by configurations

$|1^{*}2\rangle$ or $|12^{*}\rangle$ (Scheme 1). In the resulting Frenkel exciton the electronic transitions either remain localized on one of the monomer or delocalize over both monomers forming excitonic resonance states which are described as a linear combination of localized states ($|1^{*}2\rangle \pm |12^{*}\rangle$). The terms charge-separated states correspond to the situation in which the two orbitals involved in the excitation process are located on different monomers. Resulting states are described by configurations $|1^{+}2^{-}\rangle$ or $|1^{-}2^{+}\rangle$. These two states might come to resonance and form charger resonant states described as a linear combination $|1^{+}2^{-}\rangle \pm |1^{-}2^{+}\rangle$.

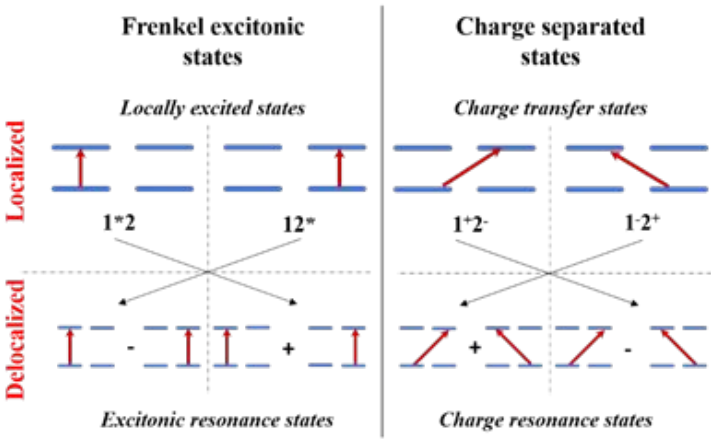


Scheme 1. Dimer excited states formed from local (left) and charge-transfer (right) transitions: localized excited states are shown on top and their linear combinations leading to delocalized states (bottom).

Despite a huge effort to understand the nature of aromatic excimers, including their optical properties, a systematic investigation of such species is still missing. In particular, the theoretical interpretations of excimer spectra formed by more extended aromatic entities are difficult due to computational demands to properly account for their character. Therefore, only excimers constructed from smaller medium-size molecules, such e.g. benzene, pyrene and perylene were addressed until now[35-38]. Modelling of these associates in their electronically excited states requires methods which properly describe the charge transfer processes, long-range electron correlations, and the higher polarizability of the excited state compared to the ground state. In addition, even monomer excited states are often of multi-configurational character and their ground state wave-function might deviate non-negligibly from the single-reference character.[39]

The reliability of Time-dependent density functional theory (TD-DFT) methods for excimer calculations, a popular choice due to their moderate computational cost, is controversial and

depends strongly on the choice of the exchange-correlation functional. Main limitations come from an incorrect description of the dispersion interactions necessary to obtain accurate ground and excited state binding energies for weakly bound van der Waals complexes,[40] and from underestimation of the electronic transition to states with considerable charge separation.[41] These limitations make the use of standard exchange-correlation functionals inappropriate for these systems. The problem has, at least partially, been overcome by the use of long-range corrected (LR) functionals being able to correct for the charge separation problems for the excited state calculations.[42] Kolaski *et al.*[38] reported on studies concerning the effect of different functionals to describe excimer properties such as binding energies and absorption and emission spectra for benzene, naphthalene, anthracene, and pyrene dimers and compared with available experimental data. The standard generalized gradient approximation Perdew–Burke–Ernzerhof (PBE) functional failed to provide reliable results for aromatic excimers larger than benzene, giving very shallow potential energy curves at the TD-DFT level and, thus, small binding energies. Significant improvements were observed with the hybrid PBE functional (PBE0) and the long-range corrected ωPBEh functional.

An interesting alternative single-reference approach to TD-DFT is the use of the algebraic diagrammatic construction to the second-order[43, 44] (ADC(2)) method which, in combination with the resolution of identity (RI),[45, 46] is a promising candidate for excited state calculations of extended aromatic complexes. This method was already proved to provide correct description of excimer properties of moderate sized systems of e.g. naphthalene[47, 48] and pyracene.[49]

The use of multi-reference wavefunction-based methods is problematic since in conventional approaches[35] the active space extensively increases with increasing size of the system. Nevertheless, medium sized naphthalene, anthracene, pyrene, and perylene excimers were investigated with the multiconfiguration quasi-degenerate perturbation theory (MCQDPT) method employing a minimal size of the complete active space of four electrons and four orbitals CAS(4e,4o).[37] The analysis of calculations using the complete active space self-consistent field (CASSCF) method have shown that the excimer formation is driven by strongly attractive intermolecular forces resulting from the mixing of CR and ER states with their almost equal contribution to the total wave function of the first excited states in the region of inter-molecular separation which corresponds to the excimer formation. The same authors recently performed studies on naphthalene excimer formation using density matrix renormalization group- complete

active space second-order perturbation theory (DMRG-CASPT2) method with a full π-orbital (20e, 20o) active space.[50] The importance of charge transfer contributions to the exciplex formation has been demonstrated recently in surface hopping dynamics studies on the benzene dimer using the RI-ADC(2) method.[36]

Alternative multi-reference (MR) description can be provided by the density functional theory/multireference configuration interaction (DFT/MRCI) method,[51] in which DFT is used to cover the dynamic electron correlation and MRCI accounts for multi-reference character of states, or the strongly contracted-*n*-electron valence state perturbation theory to second order (SC-NEVPT2).[52, 53] Both methods proved to provide accurate results of excited states of larger aromatic monomers,[39] with a better performance of the former method.

In this contribution we report on the study of the properties of electronically excited states of the PAH dimers pyrene and coronene because of their fundamental importance as has been explained above especially for the pyrene dimer. The excimer properties of larger PAHs are also of great interest for modeling purposes of the graphitic regions of CDs where larger sheets occur. Such extensions are constructed in our work by systematic circular enlargement of pyrene and coronene to circum-1-pyrene and circum-1-coronene (Figure 1). Our calculations are based on the aforementioned DFT/MRCI and SC-NEVPT2 methods for the two former systems and discuss the performance of the commonly used TD-Coulomb-attenuating method- Becke-3-Lee-Yang-Parr (TD-CAM-B3LYP) and scaled opposite-spin (SOS)-ADC(2) methods. Besides the study of UV spectra by means of the just-mentioned methods, our emphasis is laid on fluorescence spectra by focusing on geometry optimizations in the $S_1$ state. The analysis of the electronic wavefunction by means of several descriptors such as natural transition orbitals (NTOs) and charge transfer (CT) plays an important role in our discussions as well, as will be outlined in more detail below.

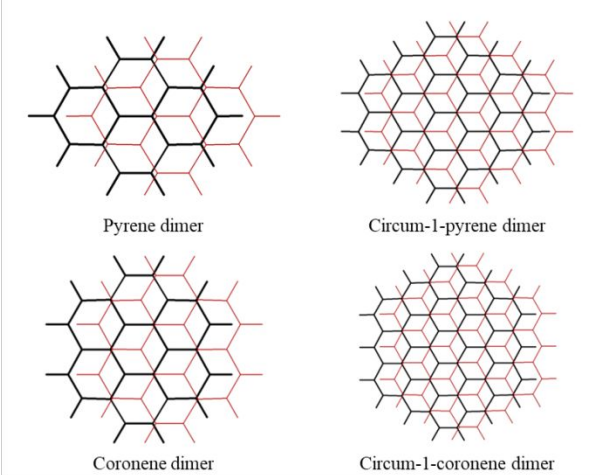


**Figure 1.** Ground state geometries of the pyrene, circum-1-pyrene, coronene, and circum-1-coronene dimers optimized with the DFT/B3LYP-D3 method (def2-TZVP basis set for pyrene and coronene, SV(P) basis set for circum-1-pyrene and circum-2-pyrene).

## 2 Computational Methods

Four stacked PAH dimers, of pyrene, circum-1-pyrene, coronene and circum-1-coronene were studied. Ground state optimized dimer geometries are shown in Figure 1. The ground-state geometries of the pyrene and coronene dimers were optimized with DFT using the three-parameter Becke, Lee-Yang-Parr (B3LYP),[54] and CAM-B3LYP[55] functionals and the SOS- second order Møller–Plesset perturbation theory (MP2)[56, 57] method using the split valence basis set (SV(P)),[58] the valence triple-ζ basis set with polarization functions (d,p) (TZVP)[59] and the triple-zeta valence polarization with (2d,f) on carbon (def2-TZVP)[60] basis sets. For the ground-state geometries of the circum-1-pyrene and circum-1-coronene dimers only the SV(P) basis was used. The SOS-MP2 and DFT-CAM-B3LYP optimized ground state geometries were used for absorption spectra calculations at the SOS-ADC(2)[43, 44] and TD-CAM-B3LYP levels, respectively. Cartesian geometries are given for selected structures and methods in the Supplementary Information (SI). Excited states were calculated at TD-DFT/CAM-B3LYP and SOS-ADC(2) levels for all dimers. The DFT/MRCI[51] and SC-NEVPT2[52, 53] multireference methods were only used for the pyrene and coronene dimers. A CAS(14,14) was used as reference space in the MR calculations for the dimers whereas for the monomers a CAS(8,8) was employed. The RI approach[45, 46] has been used for all SOS-MP2 and SOS-ADC(2) calculations.

All DFT/B3LYP, TD-B3LYP, SOS-MP2 and SOS-ADC(2) calculations were carried out in the TURBOMOLE 7.2 program.[61] The DFT and TDDFT calculations with the CAM-B3LYP functional were performed with the Gaussian 09 program.[62] The SC-NEVPT2 calculations were performed with the ORCA 4.0 package.[63] The MRCI/DFT calculations were performed with the program developed by Grimme and Waletzke[51] and extended by the group of Marian[64-66] based on DFT calculations. Becke hybrid exchange-correlation functional (BHLYP)[67] were used for the initial DFT calculations. An energy cut-off of 0.8 Hartree was used in the DFT/MRCI calculations.

The charge transfer from fragment A to fragment B using the descriptor q(CT)[48] for a given electronic transition was computed by means of transition density matrices $D^{0\alpha}$ defining the descriptor $\Omega_{AB}^{\alpha}$ as

$$\Omega_{AB}^{\alpha} = \frac{1}{2}\sum_{\substack{a \in A \\ b \in B}} \left(D^{0\alpha,[AO]} S^{[AO]}\right)_{ab} \left(S^{[AO]} D^{0\alpha,[AO]}\right)_{ab} \quad (1)$$

where α labels the electronic state and AO indicates atomic orbitals. $\Omega_{AB}^{\alpha}$ represents the contribution of charge transfer from fragment A to fragment B (for A≠B), and the contributions of the same-fragment excitations (for A = B). The total CT character for a system with multiple fragments is given by:

$$q(CT) = \frac{1}{\Omega^{\alpha}} \sum_{A} \sum_{B \neq A} \Omega_{AB}^{\alpha} \quad (2)$$

$\Omega^{\alpha}$ is the total sum of the charge transfer numbers for all pairs of A and B. If q(CT)=1$e$, a complete charge transfer of one electron has occurred while for q(CT) = 0 the transition is a locally excited or Frenkel excitonic state. This formulation allows also a convenient analysis of excimeric and CT interactions in the case of delocalized orbitals where a direct examination of the wavefunction can be cumbersome.

Natural transition orbital participation ratio ($PR_{NTO}$) values based natural transition orbitals (NTOs)[68] were calculated as:

$$PR_{NTO} = \frac{\left(\sum_i \lambda_i\right)^2}{\sum_i \lambda_i^2} \quad (3)$$

where $\lambda_i$ is the weight of each transition from hole to electron orbital. The $PR_{NTO}$ values indicate the number of essential NTOs participating and, thus, how many configurations are crucial to

describe the excited state. NTOs,[68] the $PR_{NTO}$ analysis and q(CT) values were computed for each electronic transition for the SOS-ADC(2) and TD-CAM-B3LYP calculations with the TheoDORE program[48, 69, 70].

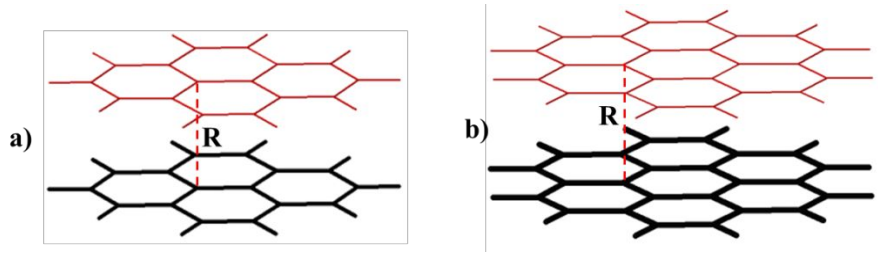


**Figure 2.** Pyrene and coronene dimer structures of a) pyrene and b) coronene, the inter sheet distance R is shown in the sideview.

## 3 Results and Discussion

Table 1 collects the interaction energies and inter sheet distances of stacked PAH dimer structures for the ground state (Figure 2) used in this study. In agreement with previous results,[71, 72] the most stable structures are parallel-displaced (AB type). As already observed previously,[71] compared to the SOS-MP2, several DFT methods significantly underestimate the interaction energies and overestimate the inter sheet distances even when the empirical dispersion corrections are included.

**Table 1.** Interaction energies ΔE and inter sheet distances of the optimized stacked dimers in the ground state.

| **Method** | **ΔE (kcal mol$^{-1}$)[d]** | **Inter sheet distance R[e]** |
|---|---|---|
| **Pyrene dimer** | | |
| SOS-MP2[a] | -14.9 | 3.35 |
| DFT/B3LYP-D3[a] | -11.8 | 3.49 |
| DFT/CAM-B3LYP-D3[a] | -10.3 | 3.52 |
| **Circum-1-pyrene dimer** | | |
| SOS-MP2[b] | -63.2 | 3.10 |

| | | |
|---|---|---|
| DFT/B3LYP-D3[b] | -44.4 | 3.37 |
| DFT/CAM-B3LYP-D3[c] | -38.5 | 3.43 |
| **Coronene dimer** | | |
| SOS-MP2[a] | -26.8 | 3.30 |
| DFT/B3LYP-D3[a] | -19.6 | 3.48 |
| DFT/CAM-B3LYP-D[a] | -17.0 | 3.52 |
| **Circum-1-coronene dimer** | | |
| SOS-MP2[b] | -88.6 | 3.15 |
| DFT/B3LYP-D3[b] | -53.8 | 3.35 |
| DFT/CAM-B3LYP-D3[c] | -51.1 | 3.42 |

[a]def2-TZVP basis set; [b]SV(P) basis set; [c]SVP basis set; [d]ΔE(dimer) = E(dimer) – 2* E(monomer)
[e] Central inter sheet C···C distance R defined in Figure 2.

## 3.1 The UV absorption spectra of the PAH dimers

**3.1.1 Pyrene dimer.** The absorption spectrum of the pyrene dimer obtained at different computational levels are compared in Figure 3. The left panel of this figure shows the bright states whereas the entire absorption spectrum is given in the right panel. CT data and a quantitative comparison of excitation energies for the lowest few states computed with different methods can be found in Table 2. Table S1 contains results on an extended set of electronic states. In Tables S1 and S2 of the SI the orbital excitation pattern of the most important configurations and $PR_{NTO}$ values are collected. They show significant multiconfigurational character ranging, e.g. in case of the analysis of the four lowest states (Table S2) at SOS-ADC(2) level from four essential configurations for the two lowest states and two for the following state. Even the HOMO/LUMO excitation shows a $PR_{NTO}$ value of 1.6 demonstrating the importance of other configurations for the description of this state. The lowest excited states result from transitions between the π-orbitals delocalized over both monomers as shown in Figure S1. In particular, monomer HOMO-1 combines in dimer as HOMO-2 and HOMO-3 and monomer highest-occupied molecular orbital (HOMO) combines in dimer as HOMO-1 and HOMO, dimer lowest unoccupied orbital (LUMO)

and LUMO+1 is a combination of monomer LUMOs and dimer LUMO+2 and LUMO+3 result from a linear combinations of the monomer (LUMO+1)s, respectively.

Early experimental studies place the absorption band of the pyrene dimer at 3.70 eV.[73, 74] The pyrene dimer is identified in free jets by a broad and unstructured band around 3.35 eV[75], in agreement with Resonance Enhanced Multi-Photon Ionization (REMPI) spectroscopy which shows a broad band with onset at 3.35 eV and a band maximum at 3.70 eV[32]. Previous calculations of the excited states of pyrene dimer were performed for both AA-type and AB-type conformers. For the former, MCQDPT calculations performed with an (4e, 4o) active space and 6-31G(d) basis set puts the first excited state at 3.66 eV[37]. Alternatively, TD-DFT calculations employing the PBE0 and long-range corrected ωPBE0 functionals and the aug-cc-pVDZ basis set result in excitation energies of 3.42 and 3.65 eV, respectively.[38] A slightly larger excitation energy of 4.02 eV was obtained with the CC2 method.[38] For the AB-type conformer the first and second excited states calculated using DFT and a TZVP basis set were found to be degenerate with an excitation energy of 3.99 eV using a BHLYP functional, and were at 3.57 and 3.82 eV with CAM-B3LYP.[32] The TD-DFT-based tight binding (TD-DFTB) method gives these energies slightly lower at 3.50 and 3.59 eV.[32] The above reported data indicate relatively large fluctuations in excitation energies obtained with various methods. In addition, the diffuse character of the observed excitation spectrum makes it difficult to set a reference value of excitation energies accurately. Based on a good agreement between the experiment and DFT/MRCI calculations observed in our previous study on absorption spectra of the monomers of polycyclic aromatic hydrocarbons[39], the present DFT/MRCI results are used as benchmark data also for the pyrene dimer.

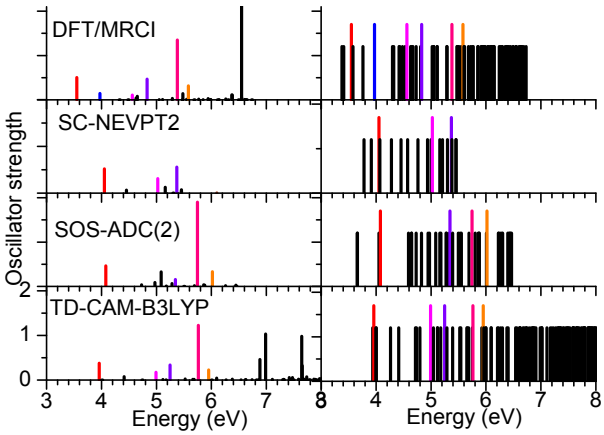


**Figure 3.** Spectrum of the pyrene dimer calculated with different methods (left: bright states with oscillator strength, right: all states with equal strength). For all SR methods the def2-TZVP basis set, and for the MR methods the SV(P) basis has been used. The same color code represents mainly the same transition type for all methods.

The first two excited states ($1^1A_u$ and $2^1A_g$) are both dark states calculated with DFT/MRCI (Table 2) and result from the combination of the lowest excited dark state $1^1B_{3u}$ ($L_b$) of the monomers with negligible shifts (less than 0.1 eV) to lower energies compared to the monomer.[39] They are split by only 0.03 eV. Inspection of the wavefunctions shows (Table S2) that both states, $1^1A_u$ and $2^1A_g$, have significant multi-configurational character. Four electronic configurations form the first and second excited states wavefunctions with all four occupied (HOMO-3 to HOMO) and all four virtual (LUMO to LUMO+3) evenly involved. The next two excited states ($2^1A_u$ and $3^1A_g$, split by 0.03 eV) are composed of combinations of the second monomer bright excited states $1^1B_{2u}$ ($L_a$) and shifted to lower excitation energies by less than 0.2 eV. The $2^1A_u$ is a bright state with the wavefunction constructed predominantly (contribution of 79%) from a HOMO/LUMO configuration. Its excitation energy of 3.55 eV agrees well with the above-mentioned experimental value of the band maximum of 3.70 eV. The $3^1A_g$ state is dark and results from HOMO/LUMO+1 and HOMO-1/LUMO transitions. Calculations performed at the SC-NEVPT2 and SOS-ADC(2) levels give a similar picture of the excited states character and energies including their shifts compared to respective monomer energies.[39] Taking into account that several excited states appear within a small energy range, some of them being almost degenerate, small differences observed in energy ordering are not surprising. The only notable difference is the character of the bright excited state labeled as $3^1A_u$ (Table 2), which has a HOMO-1/LUMO+1 character according to the SC-NEVPT2 calculations. TD-CAM-B3LYP method gives a different picture on the absorption

spectrum of pyrene dimer. In particular, $2^1A_g$, $1^1A_u$ and $3^1A_g$, $2^1A_u$ pairs are switched (see Table S2 for their wavefunction characterization). As a result, $1^1A_u$, characterized by HOMO/LUMO transition, becomes a bright state. In addition, all four excited states have significantly more charge-transfer character at the TD-CAM-B3LYP level compared to the description provided by the SOS-ADC(2) method.

SC-NEVPT2, SOS-ADC(2) and TD-CAM-B3LYP methods put the first bright excited state at ~4 eV (i.e. about 0.5 eV higher than the DFT/MRCI approach), although TD-CAM-B3LYP gives this agreement due to the wrong ordering of the bright and dark stares. All methods predict a similar oscillator strength $f$ ~0.5.

**Table 2.** Excitation energies, oscillator strengths and CT values for the lowest bright and dark excited states of the pyrene dimer calculated using several computational methods and Ci symmetry labeling.

| State no. | State | ΔE(eV) | Diff.rel. DFT/MRCI | *f* | CT |
|---|---|---|---|---|---|
| DFT/MRCI[a] | | | | | |
| 1 | $1^1$Au | 3.38 | 0.00 | 0.00 | - |
| 2 | $2^1$Ag | 3.41 | 0.00 | 0.00 | - |
| 3 | $2^1$Au | 3.55 | 0.00 | 0.50 | - |
| 4 | $3^1$Ag | 3.58 | 0.00 | 0.00 | - |
| 5 | $4^1$Ag | 3.76 | 0.00 | 0.00 | - |
| 6 | $3^1$Au | 3.97 | 0.00 | 0.14 | - |
| SC-NEVPT2[a] | | | | | |
| 1 | $2^1$Ag | 3.78 | 0.37 | 0.00 | - |
| 2 | $1^1$Au | 3.78 | 0.40 | 0.00 | - |
| 3 | $2^1$Au | 3.91 | 0.36 | 0.00 | - |
| 4 | $3^1$Au | 4.05 | 0.08 | 0.52 | - |
| SOS-ADC(2)[b] | | | | | |
| 1 | $1^1$Au | 3.66 | 0.28 | 0.00 | 0.03 |
| 2 | $2^1$Ag | 3.66 | 0.25 | 0.00 | 0.04 |
| 3 | $3^1$Ag | 4.05 | 0.47 | 0.00 | 0.03 |
| 4 | $2^1$Au | 4.08 | 0.53 | 0.46 | 0.19 |

| | | | | | |
|---|---|---|---|---|---|
| TD-CAM-B3LYP[b] | | | | | |
| 1 | $2^1Ag$ | 3.94 | 0.53 | 0.00 | 0.26 |
| 2 | $1^1Au$ | 3.96 | 0.58 | 0.38 | 0.33 |
| 3 | $3^1Ag$ | 4.00 | 0.42 | 0.00 | 0.26 |
| 4 | $2^1Au$ | 4.00 | 0.45 | 0.00 | 0.26 |

[a]SV(P) basis set; [b]def2-TZVP basis set; [c]relative to DFT/MRCI results.

**3.1.2 Circum-1-pyrene dimer.** Due to the size of the system, the calculation of the circum-1-pyrene dimer absorption spectra were performed only at the single-reference SOS-ADC(2) and TD-CAM-B3LYP levels. Results of these calculations are given in Figure 4 and Table 3. Additional information can be found in the SI (Figure S2, Table S3 and Table S4). Although the SOS-ADC(2) method overestimated the excitation energies of the first two monomer excited states by 0.4 - 0.5 eV with respect to the DFT/MRCI results[39], it still considered to provide a reliable description of the character of these states and, thus, it is primarily used for discussion on the dimer absorption spectra.

As in the case of the pyrene dimer, four lowest excited states ($2^1A_g$, $1^1A_u$, $3^1A_g$ and $2^1A_u$) result from linear combinations of the $1^1B_{3u}(^1L_b)$ and $1^1B_{2u}(^1L_a)$ monomer states, although the energy ordering in the circum-1-pyrene is different. In particular, combinations of the dark $1^1B_{3u}(^1L_b)$ monomer states form the dark $2^1A_g$ and $2^1A_u$ states, shifted by 0.12-0.15 eV, both with multi-configurational character (see Table S4 for dominant electronic contributions and $PR_{NTO}$ values). Combinations of the bright $1^1B_{2u}(^1L_a)$ monomer states form the $1^1A_u$ and $3^1A_g$ states, shifted by 0.3 and 0.2 eV respectively, the former being the bright state characterized predominantly by a HOMO/LUMO transition with the contribution of 93 % and a $PR_{NTO}$ value of 1.06 (SOS-ADC(2), Table S4). Excitation energies of all four states fall into a small energy region of 0.16 eV and, in contrast to pyrene dimer, all states have a non-negligible charge transfer character (Table 3). Different results were obtained at the TD-CAM-B3LYP level. The first two excited states $1^1A_u$ and $2^1A_g$ states result from the bright $L_a$ state. The former dimer excited state is bright and it is characterized mainly by HOMO/LUMO transition (the contribution is 94 %). The dark monomer $L_b$ states combine to give the $3^1A_g$ and $2^1A_u$ dark dimer states. In addition, a new state labeled as $4^1A_g$ of a significantly charge transfer character appears in the same energy region.

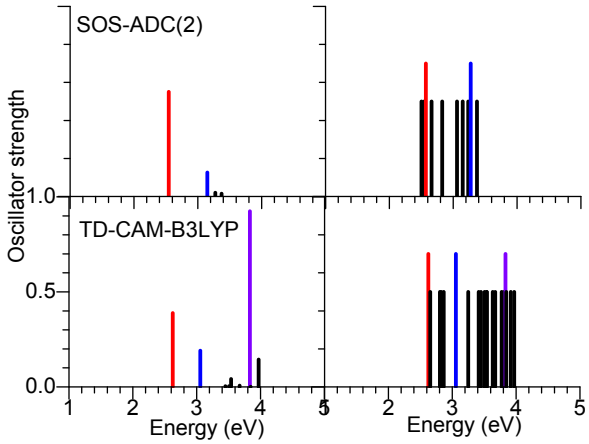


**Figure 4.** Spectrum of circum-1-pyrene dimer calculated at SOS-ADC(2)/SV(P) and TD-CAM-B3LYP/SVP level (left: bright states with oscillator strength, right: all states and with equal strength). The same color code represents mainly the same transition type for all methods**.**

**Table 3.** Excitation energies, oscillator strengths and CT values for the lowest bright and dark excited states of the circum-1-pyrene dimer calculated using several computational methods and Ci symmetry labeling

| State no. | State | ΔE(eV) | f | CT |
|---|---|---|---|---|
| SOS-ADC(2)[a] | | | | |
| 1 | $2^1$Ag | 2.50 | 0.00 | 0.29 |
| 2 | $1^1$Au | 2.54 | 0.55 | 0.37 |
| 3 | $2^1$Au | 2.57 | 0.00 | 0.26 |
| 4 | $3^1$Ag | 2.66 | 0.00 | 0.26 |
| TD-CAM-B3LYP [b] | | | | |
| 1 | $1^1$Au | 2.62 | 0.39 | 0.49 |
| 2 | $2^1$Ag | 2.66 | 0.00 | 0.22 |
| 3 | $3^1$Ag | 2.81 | 0.00 | 0.26 |
| 4 | $4^1$Ag | 2.83 | 0.00 | 0.75 |
| 5 | $2^1$Au | 2.87 | 0.00 | 0.21 |

[a]SV(P) basis set.;[b]SVP basis set.

**3.1.3 Coronene dimer.** Figure 5 and Table 4 collect the results of the coronene dimer absorption spectra calculations. The first four excited states obtained with DFT/MRCI, all with oscillator strength $f = 0$, are derived from $B_{2u}$ (2.91 eV) and $B_{3u}$ (3.44 eV)[39] monomer dark excited states.

The resulting dimer states are only negligibly shifted from monomer spectra. Analysis of the wavefunctions (see Table S6 and Figure S3) shows that all these states are of multi-configurational character with $PR_{NTO}$ values between 3-4 for the lowest four states. They involve significant contributions of eight (HOMO-3 to LUMO+3) NTO's which combine from monomer HOMO-1, HOMO, LUMO and LUMO+1 orbitals[39] . The interaction of the two monomers leads to different reordering of dimer orbitals than in the case of pyrene-based complexes. In particular, monomer HOMO-1 orbitals combine to form the dimer HOMO-1 and HOMO-2 orbitals, and monomer HOMOs form dimer HOMO and HOMO-3, respectively. Similarly, monomer LUMO and LUMO+1 orbitals form LUMO+1, LUMO+2 dimer orbitals and LUMO and LUMO+3 dimer orbitals, respectively. The first bright excited state ($3^1$Au) was calculated at 3.84 eV (Table 4) with somewhat low intensity ($f$ = 0.25) and the bright state ($10^1$Au, Table 4) with intensity comparable to the monomer spectrum ($\beta$ band at 4.1 eV, $f$ = 1.1,[39]) appears at the energy of about 4.3 eV (Figure 5 and Table 4). Excitation spectra similar to those computed with DFT/MRCI were obtained with the other methods also, including shifts of excited state energies to respective monomer excited states. The excitation energy of the first bright state ($4^1$Au in SOS-ADC(2) and $3^1$Au in CAM-B3LYP) at ~ 4.3 eV (Table 4) is, however, overestimated at the SOS-ADC(2) and TD-CAM-B3LYP level. In agreement with the DFT/MRCI method, this state has a low intensity. The first excited state with intensity comparable to that of the monomer is found in the range of 4.6 – 4.8 eV (Table 4). Note that Sanyal et al.[76, 77] found, using the TD-B3LYP method, the lowest excited state at 4.21 eV. However, in our calculations this state has very low intensity. Notably, the four lowest excited states do not show a significant charge transfer character at the SOS-ADC(2) level; it is, however, predicted slightly larger at the TD-CAM-B3LYP. Both methods agree in a nonnegligible charge transfer contribution to the higher excited states.

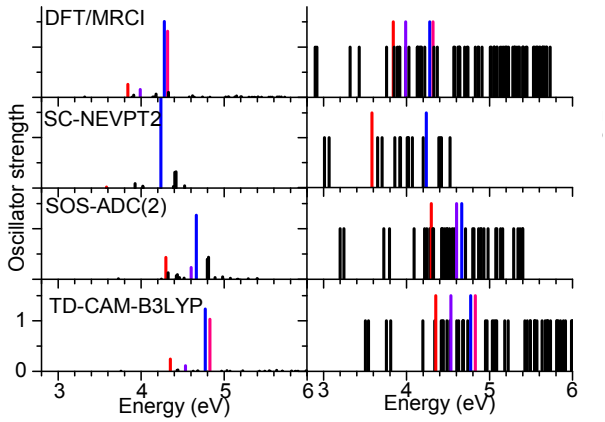


**Figure 5.** Spectrum of the coronene dimer calculated with different methods (left: bright states with oscillator strength, right: all states with equal strength). For all SR methods the def2-TZVP basis set and for the MR methods DFT/MRCI and SC-NEVPT2 the SV(P) and SVP basis sets, respectively, have been used.) The same color code represents mainly the same transition type for all methods.

**Table 4.** Excitation energies, oscillator strengths and CT values for the lowest bright and dark excited states of the coronene dimer calculated using several computational methods and Ci symmetry labeling

| State no. | State | ΔE(eV) | Diff.rel. DFT/MRCI | f | CT |
|---|---|---|---|---|---|
| DFT/MRCI[a] | | | | | |
| 1 | $1^1$Au | 2.90 | 0.0 | 0.00 | - |
| 2 | $2^1$Ag | 2.92 | 0.0 | 0.00 | - |
| 3 | $2^1$Au | 3.32 | 0.0 | 0.01 | - |
| 4 | $3^1$Ag | 3.43 | 0.0 | 0.00 | - |
| 6 | $3^1$Au | 3.84 | 0.0 | 0.26 | - |
| 21 | $10^1$Au | 4.28 | 0.0 | 1.51 | - |
| SC-NEVPT2[b] | | | | | |
| 1 | $2^1$Ag | 3.01 | 0.09 | 0.00 | |
| 2 | $1^1$Au | 3.07 | 0.17 | 0.00 | |
| 3 | $2^1$Au | 3.58 | 0.26 | 0.02 | |
| 4 | $3^1$Ag | 3.65 | 0.22 | 0.00 | |
| 8 | $3^1$Au | 3.93 | 0.09 | 0.09 | |
| 14 | $10^1$Au | 4.24 | -0.04 | 2.40 | |
| SOS-ADC(2)[c] | | | | | |

| | | | | | |
|---|---|---|---|---|---|
| 1 | $2^1Ag$ | 3.20 | 0.28 | 0.00 | 0.07 |
| 2 | $1^1Au$ | 3.25 | 0.35 | 0.00 | 0.02 |
| 3 | $2^1Au$ | 3.73 | 0.41 | 0.01 | 0.12 |
| 4 | $3^1Ag$ | 3.80 | 0.37 | 0.00 | 0.05 |
| 9 | $4^1Au$ | 4.30 | | 0.43 | 0.56 |
| 22 | $11^1Au$ | 4.67 | | 1.27 | 0.12 |
| TD-CAM-B3LYP[c] | | | | | |
| 1 | $2^1Ag$ | 3.50 | 0.58 | 0.00 | 0.26 |
| 2 | $1^1Au$ | 3.54 | 0.64 | 0.00 | 0.26 |
| 3 | $2^1Au$ | 3.76 | 0.44 | 0.00 | 0.27 |
| 4 | $3^1Ag$ | 3.81 | 0.38 | 0.00 | 0.26 |
| 7 | $3^1Au$ | 4.35 | | 0.24 | 0.45 |
| 21 | $10^1Au$ | 4.77 | 0.49 | 1.23 | 0.27 |

[a]SV(P) basis set; [b]SVP basis set; [c]def2-TZVP basis set.

**3.1.4 Circum-1-coronene dimer.** The absorption spectra of the circum-1-coronene dimer are shown in Figure 6 and Table 5. Only single-reference SOS-ADC(2) and TD-CAM-B3LYP methods were used in these calculations due to the size of the dimers. As in the case of circum-1-pyrene, the results are discussed mainly based on the data obtained by the SOS-ADC(2) method. The wavefunction and NTO analysis and $PR_{NTO}$ values (Table S8 and Figure S4) shows that the electronic transitions for the first four states mainly involve the monomer HOMO-1 to LUMO+1 NTO's. According to SOS-ADC(2) calculations, monomer HOMO's combine to dimer HOMO-1 and HOMO-2 orbitals, and HOMO-1 orbitals form HOMO and HOMO-3 dimer orbitals, respectively. The monomer LUMO and LUMO+1 orbitals form dimer pairs LUMO, LUMO+2 and LUMO+1, LUMO+3 NTO's, respectively. Similar to other complexes considered in this study, the two lowest excited states ($2^1A_g$ and $1^1A_u$) are dark states with excitation energies slightly shifted to lower values (0.21 and 0.08 eV) as compared to monomer (2.38 eV, $1^1B_{2u}$[39]) and show only relatively small contribution of charge transfer. The next pair of states ($3^1A_g$ and $2^1A_u$) are dark states also with larger charge transfer contribution. The lowest bright excited state ($3^1A_u$, Table S7) is shifted with respect to its monomer counterpart to lower energies by about 0.5 eV ($\beta$ band in the monomer at 3.4 eV, $f = 1.8$[39]). This state is placed 0.65 eV above the first excited state.

(Table S6). The TD-CAM-B3LYP results found the corresponding state with even lower intensity ($f \sim 0.3$) at excitation energy 0.5 eV higher compared to the first excited state.

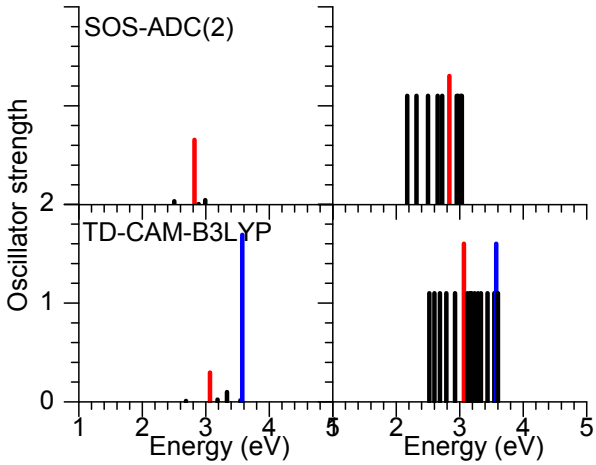


Figure 6. Spectrum of the circum-1-coronene dimer calculated at SOS-ADC(2)/SV(P) and TD-CAM-B3LYP/SVP level (left: bright states with oscillator strength, right: all states with equal strength). The same color code represents mainly the same transition type for all methods.

**Table 5.** Excitation energies, oscillator strengths and CT values for the lowest bright and dark excited states of the circum-1-coronene dimer calculated using several computational levels and Ci symmetry labeling

| State no. | State | ΔE(eV) | f | CT |
|---|---|---|---|---|
| SOS-ADC(2) [a] | | | | |
| 1 | $2^1$Ag | 2.17 | 0.00 | 0.21 |
| 2 | $1^1$Au | 2.30 | 0.00 | 0.06 |
| 3 | $2^1$Au | 2.50 | 0.03 | 0.40 |
| 4 | $3^1$Ag | 2.64 | 0.00 | 0.50 |
| TD-CAM-B3LYP [b] | | | | |
| 1 | $2^1$Ag | 2.52 | 0.00 | 0.28 |
| 2 | $1^1$Au | 2.60 | 0.00 | 0.23 |
| 3 | $2^1$Au | 2.69 | 0.01 | 0.29 |
| 4 | $3^1$Ag | 2.79 | 0.00 | 0.22 |

[a]SV(P) basis set; [b]SVP basis set.

Comparison of the results performed using both multi-reference SC-NEVPT2 and single-reference SOS-ADC(2) and TD-CAM-B3LYP methods with the benchmarking DFT/MRCI method shows different trends for pyrene and coronene. In the former case all methods put the first bright excited state slightly higher with respect to the benchmark calculations, with a similar intensity though. The ordering of states is, however, different for TD-CAM-B3LYP which places this state to among the lower ones of the absorption spectrum. For the coronene, all methods, including TD-CAM-B3LYP, give the similar trends as found at the DFT/MRCI level.

## 3.2 Emission process of PAH dimers

**3.2.1 Pyrene dimer.** Several AB-type structural displacements were used as a starting point to optimize the dimer structures in $S_1$ which resulted in three SOS-ADC(2) (For details see Figure S5 and Table S9) and two TD-CAM-B3LYP $S_1$ minima. Figure 7 shows the obtained structures which are most stable among different geometry optimizations in $S_1$ starting from different initial geometries and symmetries ($C_{2h}$ or $C_i$). Among the optimized minima at the SOS-ADC(2) level, all three structures have practically the same energy ($\Delta E_{adiab}$, Table 6). The inter sheet distance increases with an increasing overlap of the two monomers, with the differences being within 0.24 Å. The TD-CAM-B3LYP-D3 optimizations result in the graphite (AA-type, CAM-B3LYP-1) and parallel displaced AB-type (CAM-B3LYP-2) structures with the former being by 0.43 eV more stable. Also, in this case the difference in the inter sheet distances is relatively small with a difference of 0.09 Å. The spectral emission characteristics also reflect the extent of overlap between the two monomers ($\Delta E_{em}$, Table 6). The ADC(2)-2 excimer with the largest monomer overlap shows a significantly larger charge transfer character. Although adiabatic excitation energies are almost identical, the emission energies change significantly, in the range of 2.75 – 3.25 eV which is demonstrated in the emission spectra by the shift of 0.5 eV. TD-CAM-B3LYP calculations result in even larger changes. The calculated emission energies of 2.75 eV and 2.54 eV for the dimer structures with largest inter-monomer overlap (SOS-ADC(2)-2 and CAM-B3LYP-1), respectively, show quite good agreement with the experimental value of 2.59 eV.[25, 32] For comparison, single-point calculations have been performed with the DFT/MRCI method using the SOS-ADC(2) and TD-CAM-B3LYP structures, respectively (Table 6). The SOS-ADC(2)-2 structure which shows a larger monomer overlap, is now the most stable structure. Another interesting fact is the occurrence of two closely spaced states $2^1A_g$ and $1^1B_g$ for the ADC(2)-1 structure. Differences to the DFT/MRCI results are not so pronounced in case of the TD-CAM-B3LYP geometries. Our results predict that geometry fluctuations in $S_1$ which, as can be seen from the adiabatic energies, appear at a very low energy cost can be accompanied by significant changes in the emission spectra resulting in a broad emission band. Notably, the observed emission wavelength of 2.59 eV falls in the range of the reported calculated emission energies.

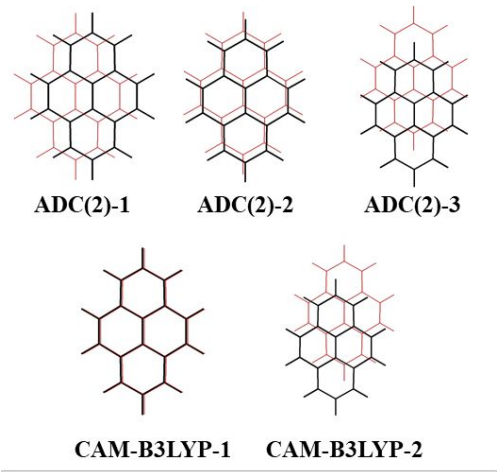


Figure 7. Different optimized pyrene dimer structures for the $S_1$ state in dependence of the initial displacement **(**SV(P) basis set and C2h symmetry was used for ADC(2)-1/3 except for ADC(2)-2, (Ci symmetry); SVP basis set and $C_1$ symmetry was used for all CAM-B3LYP cases)

**Table 6.** Inter sheet distance R (Å), adiabatic excitation and vertical $S_1$ emission energies (eV) and CT values (*e*) for the pyrene dimer calculated at different computational levels

| **SOS-ADC(2)**[a] $R(S_0)$ = 3.22 Å | | | | |
|---|---|---|---|---|
| Structure | $R(S_1)$ | $\Delta E_{adiab}$[c] | $\Delta E_{em}$[e] | CT |
| ADC(2)-1 | 3.13 | 3.46<br>*3.26*[e]<br>*3.38*[e] | 3.17<br>*2.81 ($1^1B_g$)*<br>*2.93($2^1A_g$)* | 0.18 |
| ADC(2)-2 | 3.20 | 3.47<br>*3.12*[e] | 2.75<br>*2.17($2^1A_g$)* | 0.50 |
| ADC(2)-3 | 2.96 | 3.46<br>*3.42*[e] | 3.25<br>*2.99($1^1B_g$)* | 0.17 |
| **TD-CAM-B3LYP**[b] $R_c(S_0)$ = 3.44 Å | | | | |
| Structure | $R(S_1)$ | $\Delta E_{adiab}$[c] | $\Delta E_{em}$[e] | CT |
| CAM-B3LYP-1 | 3.35 | 3.19<br>*3.14*[e] | 2.54<br>*2.46* | 0.47 |
| CAM-B3LYP-2 | 3.26 | 3.62<br>*3.44*[e] | 3.25<br>*3.07* | 0.24 |
| **Exp**. | | | 2.59[d] | |

[a]SV(P) basis set, Ci symmetry was used in all cases except for structure ADC(2)-1/3 ($C_{2h}$ symmetry).Term symbol is always $2^1A_g$ except for ADC(2)-3 ($1^1B_g$); [b]SVP basis set and $C_1$ symmetry; [c]reference energy is ground state minimum as shown in Figure 1, total energy = -1226.32229 Hartree for MP2 and - 1229.99525 Hartree for DFT/CAM-B3LYP; [d]Ref. [25, 32] .[e]DFT/MRCI energies (in italics) calculated at the respective ADC(2) and CAM-B3LYP geometry.

**3.2.2 Coronene dimer.** For the coronene dimer, by variation of the starting structures (For details see Figure S5 and Table S10), in total four optimized SOS-ADC(2) structures which are most stable among different geometry optimizations in $S_1$ starting from different initial geometries and symmetries ($C_{2h}$ or $C_i$). (Figure 8). In the ADC(2)-1, ADC(2)-2 and ADC(2)-3 structures the extent of monomer overlap is very similar; they differ primarily in the displacement directions. The displacements of the two monomers in the ADC(2)-4 structure is larger. Nevertheless, all minima have almost identical characteristics (Table 7), including the inter sheet distances (in the range of 3.16 – 3.23 Å), adiabatic excitation energies within 3.09 – 3.21 eV, and emission energies within 2.85 – 2.90 eV. The DFT/MRCI calculations performed at the SOS-ADC(2) optimized geometries give similar results for the relative stabilities (within 0.1 eV, see $\Delta E_{adiab}$ values) and emission energies of 2.55 – 2.62 eV. Respective TD-CAM-B3LYP optimized $S_1$ minima have only a slightly larger monomer overlap and all show almost identical stabilities. The inter sheet distances are larger by ~0.2 Å than the SOS-ADC(2) values. Similar to pyrene, the emission energies are shifted to higher values with respect to SOS-ADC(2) to 2.97 – 3.19 eV. Both methods predict quite small contributions of the charge transfer to excited states of all structures.

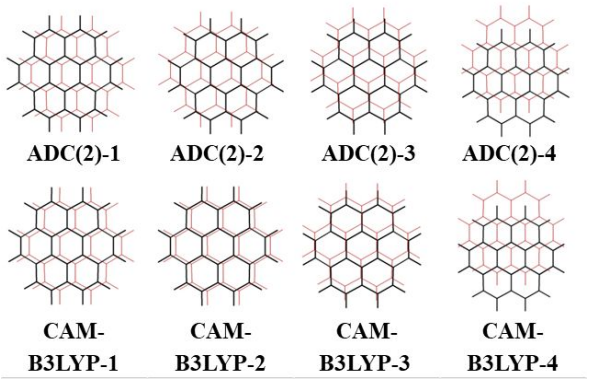


Figure 8. Different optimized coronene dimer structures for the $S_1$ state in dependence of the initial displacement (SV(P) basis set and Ci symmetry was used in all ADC(2) cases except for structure ADC(2)-1 ($C_{2h}$ symmetry), and term symbol is always $2^1A_g$; SVP basis set and $C_1$ symmetry for all CAM-B3LYP cases)

**Table 7.** Inter sheet distance R (Å), adiabatic excitation and vertical $S_1$ emission energies (eV) and CT values (*e*) for the coronene dimer calculated at different computational levels

| **SOS-ADC(2)**[a] |
|---|

| $R(S_0)$ = 3.24 Å | | | | |
|---|---|---|---|---|
| Structure | $R(S_1)$ | $\Delta E_{adiab}$[c] | $\Delta E_{em}$[d] | CT |
| ADC(2)-1 | 3.23 | 3.21<br>*2.91*[d] | 2.85<br>*2.55 ($A_g$)* | 0.20 |
| ADC(2)-2 | 3.19 | 3.10<br>*3.00*[d] | 2.89<br>*2.58 ($A_g$)* | 0.19 |
| ADC(2)-3 | 3.19 | 3.10<br>*2.99*[d] | 2.87<br>*2.56 ($A_g$)* | 0.20 |
| ADC(2)-4 | 3.16 | 3.09<br>*2.99*[d] | 2.90<br>*2.62 ($A_g$)* | 0.17 |
| **TD-CAM-B3LYP[b]**<br>$R(S_0)$ = 3.45 Å | | | | |
| Structure | $R(S_1)$ | $\Delta E_{adiab}$[c] | $\Delta E_{em}$[d] | CT |
| CAM-B3LYP-1 | 3.38 | 3.33 | 3.03 | 0.24 |
| CAM-B3LYP-2 | 3.42 | 3.33 | 2.97 | 0.18 |
| CAM-B3LYP-3 | 3.38 | 3.32 | 3.02 | 0.18 |
| CAM-B3LYP-4 | 3.30 | 3.34 | 3.19 | 0.15 |

[a]SV(P) basis set, $C_i$ symmetry was used in all cases except for structure ADC(2)-1 ($C_{2h}$ symmetry). Term symbol is always $2^1A_g$; [b]SVP basis set and $C_1$ symmetry; [c]reference energy is ground state minimum as shown in Figure 1, total energy = - 1836.08180 Hartree for MP2 and - 1841.50193 for DFT/CAM-B3LYP; [d] DFT/MRCI results (in italics) at the respective ADC(2) and CAM-B3LYP geometry.

**3.2.3 Circum-1-pyrene dimer.** In the optimizations of the $S_1$ structure of circum-1-pyrene, only one energy minimum each was located at SOS-ADC(2) and TD-CAM-B3LYP levels (Figure 9). Table 8 collects the obtained results. The inter sheet distance is about 0.3 Å smaller in the SOS-ADC(2) calculation. Both methods give almost identical adiabatic excitation and emission energies of 2.3 and 1.9 eV ($\lambda_{em}$ ~ 640 nm), respectively. The charge transfer character of the $S_1$ state (q(CT) ~ 0.4 *e*) is also quite significant.

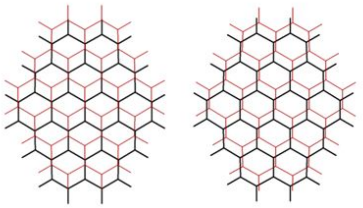


Figure 9. Different optimized circum-1-pyrene dimer structures for the $S_1$ state in dependence of the initial displacement (SV(P) basis set and Ci symmetry was used in all ADC(2) cases and term symbol is always $2^1A_g$; SVP basis set and $C_1$ symmetry was used in all CAM-B3LYP cases.)

**Table 8.** Inter sheet distance R (Å), adiabatic excitation and vertical $S_1$ emission energies (eV) and CT values (*e*) for the circum-1-pyrene dimer calculated at different computational levels

| **SOS-ADC(2)**[a] $R(S_0)$ = 3.10 Å | | | | |
|---|---|---|---|---|
| Structure | $R(S_1)$ | $\Delta E_{adiab}$[c] | $\Delta E_{em}$ | CT |
| ADC(2)-1 | 3.08 | 2.32 | 1.93 | 0.38 |
| **TD-CAM-B3LYP**[b] $R(S_0)$ = 3.43 Å | | | | |
| Structure | $R(S_1)$ | $\Delta E_{adiab}$ | $\Delta E_{em}$ | CT |
| CAM-B3LYP-1 | 3.37 | 2.31 | 1.92 | 0.36 |

[a]SV(P) basis set, Ci symmetry was used in all cases and term symbol is always $2^1A_g$; [b]SVP basis set and $C_1$ symmetry; [c]reference energy is ground state minimum as shown in Figure 1, total energy = - 3207.43239 Hartree for MP2 and -3216.75252 Hartree for DFT/CAM-B3LYP.

**3.2.4 Circum-1-coronene dimer.** Two minima were located on the $S_1$ surface (Figure 10) with both the SOS-ADC(2) and TD-CAM-B3LYP methods. The two structures differ in the geometrical monomer overlap. Based on adiabatic energies (Table 9), the ADC(2)-1 structure, which shows the larger overlap, is found to be more stable than ADC(2)-2 whereas for TD-CAM-B3LYP the reverse ordering by almost the same energy is found. The differences between the energies of the two structures are, however, only ~0.07 eV. The emission energy computed at SOS-ADC(2) is larger for the lower energy structure ADC(2)-1 by ~0.2 eV in relation to ADC(2)-2 which indicates differences in the ground state energies at the two geometries. For TD-CAM-B3LYP, the order of the stabilities and the emission energies is the same.

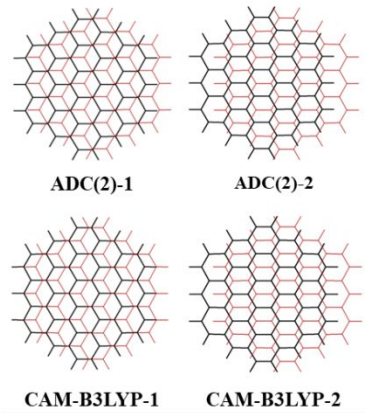


Figure 10. Different optimized circum-1-coronene dimer structures for the $S_1$ state in dependence of the initial displacement **(**SV(P) basis set and Ci symmetry was used in all ADC(2) cases and term symbol is always $2^1A_g$; SVP basis set and $C_1$ symmetry was used in all CAM-B3LYP cases.)

**Table 9.** Inter sheet distance R (Å), adiabatic excitation and vertical $S_1$ emission energies (eV) and CT values (*e*) for the circum-1-coronene dimer calculated at different computational levels

| **SOS-ADC(2)**[a] $R(S_0) = 3.14$ | | | | |
|---|---|---|---|---|
| Structure | $R(S_1)$ | $\Delta E_{adiab}$[c] | $\Delta E_{em}$ | CT |
| ADC(2)-1 | 3.11 | 2.13 | 2.07 | 0.25 |
| ADC(2)-2 | 3.08 | 2.20 | 1.85 | 0.31 |
| **TD-CAM-B3LYP**[b] $R(S_0) = 3.43$ | | | | |
| Structure | $R(S_1)$ | $\Delta E_{adiab}$[c] | $\Delta E_{em}$ | CT |
| CAM-B3LYP-1 | 3.36 | 2.46 | 2.34 | 0.26 |
| CAM-B3LYP-2 | 3.35 | 2.38 | 2.24 | 0.30 |

[a]SV(P) basis set, $C_i$ symmetry was used in all cases. Term symbol is always $2^1A_g$; [b]SVP basis set and $C_1$ symmetry; [c]reference energy is ground state minimum as shown in Figure 1; total energy = -4120.92793 Hartree for MP2 and -4132.82842 for DFT/CAM-B3LYP.

The results on the dimer emission spectra calculations show similar trends for all systems. The TD-CAM-B3LYP-D3 method gives the structures with larger inter sheet distances and tends to provide structures with larger overlap in their monomer mutual orientation. Despite this difference, both methods give excimer structures with similar stabilities (i.e. vertical adiabatic energies) and emission in a similar energy region.

## Conclusion

The absorption and emission spectra of pyrene and coronene have been calculated by means of multi-reference DFT/MRCI and NEVPT2 and single-reference SOS-ADC(2) and TD-CAM-B3LYP methods. For the circular extended derivatives, circum-1-pyrene and circum-1-coronene, the two single-reference methods have been used. Based on the good agreement between DFT/MRCI and experimental data on the pyrene dimer absorption spectrum and the previously reported monomer calculations,[39] the DFT/MRCI method served as benchmark for methods employed for larger the systems. SOS-ADC(2) and TD-CAM-B3LYP methods overestimated excitation energies by a margin of 0.3 to 0.6 eV, with the largest deviations belonging to the TD-CAM-B3LYP method. This method produces in principle a reasonable list of lowest excited states, but fails to provide a correct ordering of the bright and dark states (pyrene) and tends to underestimate excitation energies of charge transfer states (circum-1-pyrene). The results indicate the multi-configurational character of most excited states, as seen from the results of $PR_{NTO}$ analyses. The absorption energies decrease with increasing size of system; the positions of bright states are, however, different in pyrene- and coronene-based systems. While the first bright state appears within the four lowest excited states in the case of pyrene-based molecules, the number of dark states placed below the first bright state is significantly higher in the case of coronene-based molecules.

To address the topic of fluorescence emission processes, $S_1$ geometry optimizations have been performed using single-reference ADC(2)-SOS and TD-CAM-B3LYP methods for which analytic excited-state energy gradients were available. Among the whole series, the inter sheet distances are slightly larger in the optimized structures performed with TD-CAM-B3LYP method. This distance lies in the ranges of 3.0 – 3.2 Å and 3.2 – 3.4 Å for structures optimized at the ADC(2)-SOS and TD-CAM-B3LYP levels, respectively. Inter sheet distances for the $S_1$ state decrease in comparison to the corresponding ground-state values. These reductions are largest for the pyrene dimer and can amount to ~0.1 Å, depending on the case. For the remaining dimers the interring bond shortenings are much smaller, mostly only a few hundredths of an Å. Based on this observation we conclude that the inter-sheet distances of excimers/dimers will reach the intersheet limit similar to values found for circum-1-pyrene and circum-1-coronene when extending the sheet size corresponding to carbon dots. Several $S_1$ minima have been found and the largest variability in emission energies is observed for pyrene. DFT/MRCI calculations confirm this observation. Such variability can be explained by larger shortening of the monomer separation when going from

the ground state to excited state minima of pyrene. The character of the ground-state PES is more sensitive to the mutual monomer orientation at shorter distances (repulsive part of the ground state PES) which significantly influences the resulting emission energies. As already mentioned just before, the changes in monomer distances are less pronounced in the other systems and, thus, the emission spectra are more regular. The red-shift between the absorption and emission spectra depends on the shape of the structure, in particular, it is smaller for more regular coronene-based structures. Trends observed in the emission spectra led us to predict that the red-shift will die out with increasing system size as well as that the emission energy will reach its limit for carbon dots. Comparison with experimental fluorescence energies can be made in the case of the pyrene dimer. Our results indicated shallow regions of the $S_1$ energy so that no unique assignment of the experimental transition to a specific geometry could be made. Nevertheless, the experimental emission energy is found to be within the range of the computed ones. The structure with the closest agreement with the experimental value is the one with the biggest geometrical overlap of the two pyrene sheets. In this transition a notable CT of ~0.5 *e* was computed also.

Based on the multi-configurational character of the system, the multi-reference DFT/MRCI method, when computationally feasible, is recommended for calculations of optical properties for PAH-dimers. Single-reference SOS-ADC(2) and TD-CAM-B3LYP methods provide reasonably good results, the latter, however, has some difficulties to always correctly describe the ordering of states and, thus, should be carefully checked.

## Conflicts of interest

There are no conflicts to declare.

## Acknowledgments

We are grateful for generous support by the School of Pharmaceutical Science and Technology, Tianjin University, Tianjin, China, including computer time on the SPST computer cluster Arran. DN acknowledges the support from research project RVO (61388963) of the IOCB of the CAS and of the Czech Science Foundation (GA16-16959S). FBCM gratefully acknowledges the financial assistance of the Brazilian agencies Conselho Nacional de Desenvolvimento Científico e Tecnológico (CNPq) under Projects Nos. 307052/2016-8, 404337/2016-3, Fundação de Amparo à Pesquisa do Estado de São Paulo (FAPESP) under Project No. 2017/07707-3 and Coordenação de Aperfeiçamento de Pessoal de Nível Superior (CAPES) under Project CAPES/PVE Project No. 8881.066022/2014-01. FBCM, AJAA and HL are thankful to the FAPESP/Tianjin University SPRINT program (project no. 2017/50157-4) for travel support. This work was supported by the Center for Integrated Nanotechnologies (Project No. C2013A0070), an Office of Science User Facility operated for the U.S. Department of Energy Office of Science by Los Alamos National Laboratory (Contract DE-AC52-06NA25396) and Sandia National Laboratories (Contract DE-AC04-94AL85000).

## References


1. J. Gu, M. J. Hu, Q. Q. Guo, Z. F. Ding, X. L. Sun and J. Yang, *Rsc Adv.*, 2014, **4**, 50141-50144.
2. S. Y. Lim, W. Shen and Z. Q. Gao, *Chem. Soc. Rev.*, 2015, **44**, 362-381.
3. J. Zhang and S. H. Yu, *Mater. Today*, 2016, **19**, 382-393.
4. K. Hola, Y. Zhang, Y. Wang, E. P. Giannelis, R. Zboril and A. L. Rogach, *Nano Today*, 2014, **9**, 590-603.
5. M. K. Barman and A. Patra, *J. Photochem. Photobiol., C*, 2018, **37**, 1-22.
6. L. Xiao and H. D. Sun, *Nanoscale Horiz.*, 2018, **3**, 565-597.
7. V. C. Hoang, M. Hassan and V. G. Gomes, *Appl. Mater. Today*, 2018, **12**, 342-358.
8. K. Hola, M. Sudolska, S. Kalytchuk, D. Nachtigallova, A. L. Rogach, M. Otyepka and R. Zboril, *ACS Nano*, 2017, **11**, 12402-12410.
9. D. Gao, H. Zhao, X. Chen and H. Fan, *Materials Today Chemistry*, 2018, **9**, 103-113.
10. M. Shamsipur, A. Barati, A. A. Taherpour and M. Jamshidi, *J. Phys. Chem. Lett.*, 2018, **9**, 4189-4198.
11. X. Yan, X. Cui and L. S. Li, *J. Am. Chem. Soc.*, 2010, **132**, 5944-5945.
12. S. Zhu, Y. Song, X. Zhao, J. Shao, J. Zhang and B. Yang, *Nano Research*, 2015, **8**, 355-381.
13. T. Förster, *Angew. Chem., Int. Ed. Engl.*, 1969, **8**, 333-343.
14. W. Klöpffer, in *Organic Molecular Photophysics, Birks, JB, Ed.,* 1973, pp. 357-402.
15. J. Vollbrecht, *New J. Chem.*, 2018, **42**, 11249-11254.
16. L. M. Veca, A. Diac, I. Mihalache, P. Wang, G. E. LeCroy, E. M. Pavelescu, R. Gavrila, E. Vasile, A. Terec and Y.-P. Sun, *Chem. Phys. Lett.*, 2014, **613**, 40-44.
17. J. L. Wang, F. Zhang, Y. L. Wang, Y. Z. Yang and X. G. Liu, *Carbon*, 2018, **126**, 426-436.
18. Z. C. Liang, M. J. Kang, G. F. Payne, X. H. Wang and R. C. Sun, *Acs Applied Materials & Interfaces*, 2016, **8**, 17478-17488.
19. T. Aida, E. W. Meijer and S. I. Stupp, *Science*, 2012, **335**, 813-817.
20. V. Percec, M. Glodde, T. K. Bera, Y. Miura, I. Shiyanovskaya, K. D. Singer, V. S. K. Balagurusamy, P. A. Heiney, I. Schnell, A. Rapp, H. W. Spiess, S. D. Hudson and H. Duan, *Nature*, 2002, **419**, 384-387.
21. Y. M. Sun, G. C. Welch, W. L. Leong, C. J. Takacs, G. C. Bazan and A. J. Heeger, *Nat. Mater.*, 2012, **11**, 44-48.
22. M. Sudolska, M. Dubecky, S. Sarkar, C. J. Reckmeier, R. Zboril, A. L. Rogach and M. Otyepka, *J. Phys. Chem. C* 2015, **119**, 13369-13373.
23. S. Sarkar, M. Sudolska, M. Dubecky, C. J. Reckmeier, A. L. Rogach, R. Zboril and M. Otyepka, *J. Phys. Chem. C* 2016, **120**, 1303-1308.
24. G. D. Scholes, *Adv. Funct. Mater.*, 2008, **18**, 1157-1172.
25. T. Förster and K. Kasper, *Elektrochem.* , 1955, **59**, 976-980.
26. T. M. Figueira-Duarte and K. Mullen, *Chem. Rev.*, 2011, **111**, 7260-7314.
27. J. B. Birks, D. J. Dyson, I. H. Munro and F. B. Hilton, *Proc. R. Soc. London A* 1963, **275**, 575-588.
28. J. B. Birks, M. D. Lumb, I. H. Munro and F. B. Hilton, *Proc. R. Soc. London A* 1964, **280**, 289-297.
29. F. M. Winnik, *Chem. Rev.*, 1993, **93**, 587-614.
30. T. Förster, *Pure Appl. Chem*, 1962, **4**, 121-134.
31. R. D. Pensack, R. J. Ashmore, A. L. Paoletta and G. D. Scholes, *J. Phys. Chem. C* 2018, **122**, 21004-21017.
32. J. Hoche, H. C. Schmitt, A. Humeniuk, I. Fischer, R. Mitric and M. I. S. Rohr, *Phys. Chem. Chem. Phys.*, 2017, **19**, 25002-25015.
33. G. D. Scholes and K. P. Ghiggino, in *Advances in Multi-Photon Processes and Spectroscopy*, pp. 95-331.
34. A. L. L. East and E. C. Lim, *J. Chem. Phys.*, 2000, **113**, 8981-8994.
35. H. Lischka, D. Nachtigallova, A. J. A. Aquino, P. G. Szalay, F. Plasser, F. B. C. Machado and M. Barbatti, *Chem. Rev.*, 2018, **118**, 7293-7361.
36. T. M. Cardozo, A. P. Galliez, I. Borges, F. Plasser, A. J. A. Aquino, M. Barbatti and H. Lischka, *Phys. Chem. Chem. Phys.*, 2019, in press.
37. S. Shirai, S. Iwata, T. Tani and S. Inagaki, *J. Phys. Chem. A* 2011, **115**, 7687-7699.
38. M. Kolaski, C. R. Arunkumar and K. S. Kim, *J. Chem. Theory Comput.*, 2013, **9**, 847-856.
39. B. Shi, D. Nachtigallová, A. J. A. Aquino, F. B. C. Machado and H. Lischka, *J. Chem. Phys.*, submitted.
40. S. Tsuzuki and H. P. Luthi, *J. Chem. Phys.*, 2001, **114**, 3949-3957.
41. A. Dreuw, J. L. Weisman and M. Head-Gordon, *J. Chem. Phys.*, 2003, **119**, 2943-2946.
42. A. W. Lange, M. A. Rohrdanz and J. M. Herbert, *J. Phys. Chem. B*, 2008, **112**, 6304-6308.
43. J. Schirmer, *Phys. Rev. A*, 1982, **26**, 2395-2416.
44. A. B. Trofimov and J. Schirmer, *J. Phys. B: At., Mol. Opt. Phys.*, 1995, **28**, 2299.
45. C. Hattig and F. Weigend, *J. Chem. Phys.*, 2000, **113**, 5154-5161.
46. A. Kohn and C. Hattig, *J. Chem. Phys.*, 2003, **119**, 5021-5036.
47. M. Pabst, B. Lunkenheimer and A. Kohn, *J. Phys. Chem. C* 2011, **115**, 8335-8344.
48. F. Plasser and H. Lischka, *J. Chem. Theory Comput.*, 2012, **8**, 2777-2789.

49. J. Auerswald, B. Engels, I. Fischer, T. Gerbich, J. Herterich, A. Krueger, M. Lang, H. C. Schmitt, C. Schon and C. Walter, *Phys. Chem. Chem. Phys.*, 2013, **15**, 8151-8161.
50. S. Shirai, Y. Kurashige and T. Yanai, *J. Chem. Theory Comput.*, 2016, **12**, 2366-2372.
51. S. Grimme and M. Waletzke, *J. Chem. Phys.*, 1999, **111**, 5645-5655.
52. C. Angeli, R. Cimiraglia and J. P. Malrieu, *Chem. Phys. Lett.*, 2001, **350**, 297-305.
53. C. Angeli, R. Cimiraglia and J. P. Malrieu, *J. Chem. Phys.*, 2002, **117**, 9138-9153.
54. A. D. Becke, *J. Chem. Phys.*, 1993, **98**, 5648-5652.
55. T. Yanai, D. P. Tew and N. C. Handy, *Chem. Phys. Lett.*, 2004, **393**, 51-57.
56. C. Møller and M. S. Plesset, *Phys. Rev.*, 1934, **46**, 618-622.
57. Y. Jung, R. C. Lochan, A. D. Dutoi and M. Head-Gordon, *J. Chem. Phys.*, 2004, **121**, 9793-9802.
58. A. Schäfer, H. Horn and R. Ahlrichs, *J. Chem. Phys.*, 1992, **97**, 2571-2577.
59. A. Schäfer, C. Huber and R. Ahlrichs, *J. Chem. Phys.*, 1994, **100**, 5829-5835.
60. F. Weigend and R. Ahlrichs, *Phys. Chem. Chem. Phys.*, 2005, **7**, 3297-3305.
61. R. Ahlrichs, M. Bär, M. Häser, H. Horn and C. Kölmel, *Chem. Phys. Lett.*, 1989, **162**, 165-169.
62. M. J. Frisch, G. W. Trucks, H. B. Schlegel, G. E. Scuseria, M. A. Robb, J. R. Cheeseman, G. Scalmani, V. Barone, G. A. Petersson, H. Nakatsuji, X. Li, M. Caricato, A. Marenich, J. Bloino, B. G. Janesko, R. Gomperts, B. Mennucci, H. P. Hratchian, J. V. Orti, A. F. Izmaylov, J. L. Sonnenber, D. Williams-Young, F. Din, F. Lipparin, F. Egidi, J. Goings, B. Peng, A. Petrone, T. Henderson, D. Ranasinghe, V. G. Zakrzewski, J. Gao, N. Rega, G. Zheng, W. Liang, M. Hada, M. Ehara, K. Toyota, R. Fukuda, J. Hasegawa, M. Ishida, T. Nakajima, Y. Honda, O. Kitao, H. Nakai, T. Vreven, K. Throssell, J. A. Montgomery, Jr., J. E. Peralta, F. Ogliaro, M. Bearpar, J. J. Heyd, E. Brothers, K. N. Kudin, V. N. Staroverov, T. Keith, R. Kobayashi, J. Normand, K. Raghavachari, A. Rendel, J. C. Buran, S. S. Iyengar, J. Tomasi, M. Cossi, J. M. Millam, M. Klene, C. Adamo, R. Cammi, J. W. Ochtersk, R. L. Martin, K. Morokuma, O. Farkas, J. B. Foresman and D. J. Fox, *GAUSSIAN 09 (Revision A.02)*, Inc., Wallingford, CT, 2009.
63. F. Neese, *Wires Comput. Mol. Sci.*, 2018, **8**, e1327.
64. I. Lyskov, M. Kleinschmidt and C. M. Marian, *J. Chem. Phys.*, 2016, **144**, 034104.
65. A. Heil, M. Kleinschmidt and C. M. Marian, *J. Chem. Phys.*, 2018, **149**, 164106.
66. C. M. Marian, A. Heil and M. Kleinschmidt, *Wiley Interdiscip. Rev.: Comput. Mol. Sci.*, online https://doi.org/10.1002/wcms.1394.
67. A. D. Becke, *J. Chem. Phys.*, 1993, **98**, 1372-1377.
68. R. L. Martin, *J. Chem. Phys.*, 2003, **118**, 4775-4777.
69. F. Plasser, S. A. Bappler, M. Wormit and A. Dreuw, *J. Chem. Phys.*, 2014, **141**, 024107.
70. F. Plasser, TheoDORE: a package for theoretical density, orbital relaxation, and exciton analysis; available from http://theodore-qc.sourceforge.net/.
71. N. J. Silva, F. B. C. Machado, H. Lischka and A. J. A. Aquino, *Phys. Chem. Chem. Phys.*, 2016, **18**, 22300-22310.
72. R. Podeszwa and K. Szalewicz, *Phys. Chem. Chem. Phys.*, 2008, **10**, 2735-2746.
73. T. Azumi and S. P. McGlynn, *J. Chem. Phys.*, 1964, **41**, 3131-3138.
74. J. B. Birks, I. H. Munro and D. J. Dyson, *Proc. R. Soc. London, Ser. A*, 1963, **275**, 575-588.
75. Y. Numata, T. Nirasawa and I. Suzuka, *J. Photochem. Photobiol., A*, 2010, **209**, 27-31.
76. S. Sanyal, A. K. Manna and S. K. Pati, *J. Phys. Chem. C* 2013, **117**, 825-836.
77. S. Sanyal, A. K. Manna and S. K. Pati, *J. Mater. Chem. C*, 2014, **2**, 2918-2928.